Filtration of submicrometer particles by pelagic tunicates

Kelly R. Sutherland[a,1,2], Laurence P. Madin[a], and Roman Stocker[b]

[a]Biology Department, Woods Hole Oceanographic Institution, Woods Hole, MA 02543; and [b]Parsons Laboratory, Department of Civil and Environmental Engineering, Massachusetts Institute of Technology, Cambridge, MA 02139

Edited by Mimi A. R. Koehl, University of California, Berkeley, CA, and approved July 14, 2010 (received for review March 17, 2010)

Salps are common in oceanic waters and have higher per-individual filtration rates than any other zooplankton filter feeder. Although salps are centimeters in length, feeding via particle capture occurs on a fine, mucous mesh (fiber diameter d ~0.1 μm) at low velocity (U = 1.6 ± 0.6 cm·s^{-1}, mean ± SD) and is thus a low Reynolds-number (Re ~10^{-3}) process. In contrast to the current view that particle encounter is dictated by simple sieving of particles larger than the mesh spacing, a low-Re mathematical model of encounter rates by the salp feeding apparatus for realistic oceanic particle-size distributions shows that submicron particles, due to their higher abundances, are encountered at higher rates (particles per time) than larger particles. Data from feeding experiments with 0.5-, 1-, and 3-μm diameter polystyrene spheres corroborate these findings. Although particles larger than 1 μm (e.g., flagellates, small diatoms) represent a larger carbon pool, smaller particles in the 0.1- to 1-μm range (e.g., bacteria, *Prochlorococcus*) may be more quickly digestible because they present more surface area, and we find that particles smaller than the mesh size (1.4 μm) can fully satisfy salp energetic needs. Furthermore, by packaging submicrometer particles into rapidly sinking fecal pellets, pelagic tunicates can substantially change particle-size spectra and increase downward fluxes in the ocean.

biofiltration | low Reynolds number | salps | colloids | carbon cycle

Filter feeding is a common strategy among marine plankton for collecting small food particles from a suspension. Pelagic tunicates in the class Thaliacea, order Salpida, have the highest per-individual filtration rates of all marine zooplankton filter feeders (1). Weight-specific clearance rates (70–4,153 mL·mg$_C^{-1}$·h^{-1}) (2) are higher than most copepod and krill species. Salps filter feed by rhythmically pumping water into the oral siphon, through the pharyngeal chamber, and out the atrial siphon (Fig. 1*A*). This pumping action, generated by circular muscle bands, also creates a propulsive jet for locomotion. Food particles entering the pharyngeal chamber are strained through a mucous net that is continuously secreted and rolled into a food strand that moves posteriorly toward the esophagus. The bag-like net is secreted by the endostyle and fills much of the pharyngeal chamber (Fig. 1*A*). This feeding mechanism results in ingestion of any particles that enter the atrial siphon and adhere to the filtering mesh.

After digestion, particles are packaged into dense fecal pellets, which often contain undigested or partially digested plankton (3, 4). These pellets remain intact for days (4) and have sinking speeds (200–3,646 m·d^{-1}) (5, 6) that are higher than most copepod or krill pellets (3). Furthermore, diurnal vertical migration by some species may accelerate vertical export (7, 8). The combination of high filtration rates, small mesh size, and rapid pellet sinking implies that salps have the potential to shift particle distributions toward larger sizes, contribute to vertical transport, and remove substantial amounts of primary production from surface waters. These impacts will be particularly profound following population increases, which can occur suddenly under favorable conditions due to short generation times and a two-part life cycle comprising asexually reproducing individuals and pseudocolonial chains of sexually reproducing salps (1).

Generally, encounter rates between particles and filter elements depend on the Reynolds number (Re = dU/ν, where d is mesh fiber diameter, U is velocity, and ν is kinematic viscosity), which measures the relative importance of inertial and viscous forces. At low Re (Re << 1), viscous effects prevail and prevent flow separation around filter elements (9). Filtration in salps operates in this regime, as Re ~2×10^{-3}, based on mesh fiber diameter (d ~ 0.1 μm) (10), velocity at the mesh (U = 1.6 ± 0.6 cm·s^{-1}; mean ± SD), and seawater viscosity (ν = 0.83×10^{-6} m^2·s^{-1}). Classic principles of low-Re filtration theory (9, 11) show that low-Re filter feeders can collect particles smaller than the mesh spacing by relying on mechanisms other than simple sieving. The primary mechanisms are direct interception of particles traveling on streamlines that come within one particle radius of the filter element, and diffusional deposition caused by Brownian effects or random motility, which deflect particles from streamlines and cause contact with the filter. Theoretical models of caddisfly larvae (12, 13) and experiments on marine appendicularians (14–16) showed encounter of particles much smaller than the mesh size via diffusional deposition and direct interception, and theory suggests that other encounter mechanisms (inertial impaction and gravitational deposition) are negligible for most marine filter-feeders (13, 17, 18). The transition from encounter to capture depends on the sticking coefficient α, which represents the fraction of encountered particles that is captured.

Empirical studies of salp retention efficiency found a size retention cutoff of 1–2 μm, but this remains inconclusive because submicrometer particles were neglected (4, 19) or undetectable (20). In fact, small cyanobacteria (0.7–1 μm) have been removed by salps during feeding studies (20) and identified in salp fecal pellets (3, 4). Because the smallest particles are the most abundant in the ocean (Fig. 1*B*) (29, 30), determining the encounter efficiency of submicrometer particles is of particular importance to quantify clearance rates and vertical transport of particulates. Contrary to the current understanding that salps do not retain particles below 1–2 μm, we show that salps can capture submicrometer particles, and do so at rates that exceed those of larger particles. We calculate that salps can fulfill their energetic requirements with particles smaller than the mesh width and propose that they can substantially influence particle-size spectra in the upper ocean, increasing particle size and thus accelerating vertical transport of particulate matter.

Author contributions: K.R.S, L.P.M., and R.S. designed research; K.R.S., L.P.M., and R.S. performed research; K.R.S. analyzed data; and K.R.S, L.P.M., and R.S. wrote the paper.

The authors declare no conflict of interest.

This article is a PNAS Direct Submission.

[1]To whom correspondence should be addressed. E-mail: krsuth@caltech.edu.

[2]Present address: Department of Bioengineering, California Institute of Technology, East California Boulevard, Pasadena, CA 91125.

This article contains supporting information online at www.pnas.org/lookup/suppl/doi:10.1073/pnas.1003599107/-/DCSupplemental.

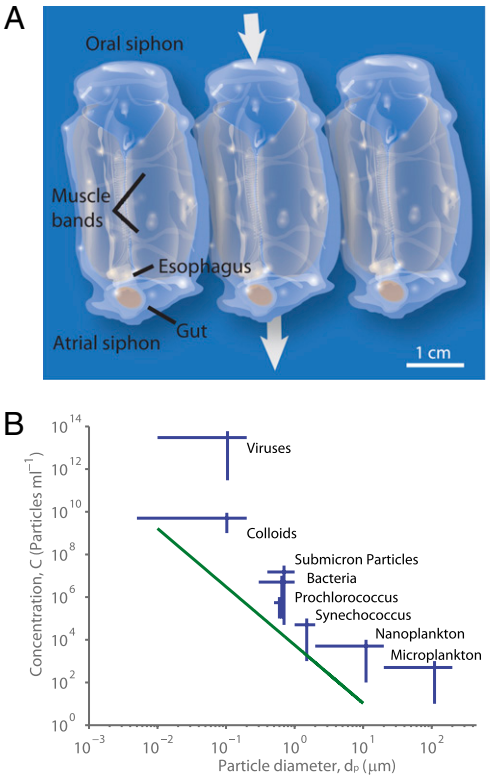

Fig. 1. Pelagic tunicates and particulate food. (*A*) Schematic of three *Pegea confoederata* individuals (aggregate stage). Mucous feeding filter (normally transparent) is shaded in red, and direction of feeding current shown with arrows. (*B*) Size distribution of living and nonliving particles in the upper ocean, including viruses (21), colloids (22), submicron particles (23), bacteria (24, 25), *Prochlorococcus* (26), *Synechococcus* (25), nanoplankton (24, 27), and microplankton (24, 27). Line is regression of microphytoplankton concentration vs. cell diameter, $\log_{10}C = -0.91\ \log_{10}(d_P^3\ \pi/6) + 3.5$; C (particles·mL^{-1}), d_P (μm) (28). Graphic by E. P. Oberlander, Woods Hole Oceanographic Institution.

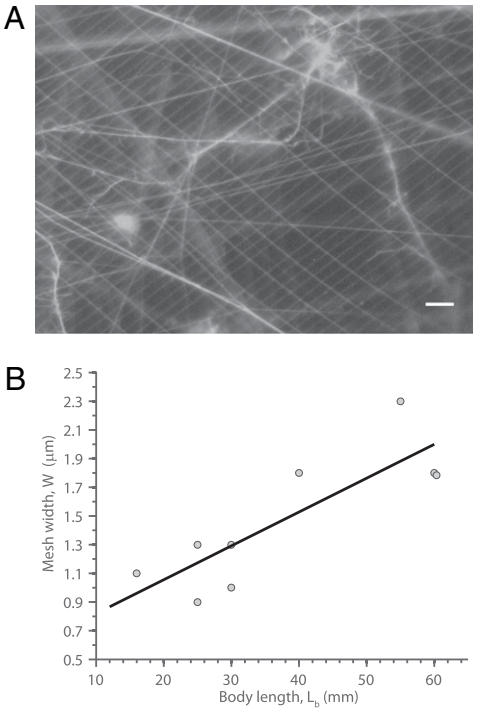

Fig. 2. Filtering mesh of *P. confoederata*. (*A*) Epifluorescent image of mesh. (Scale bar: 5 μm.) (*B*) Mesh width, W (μm), as a function of body length, L_b (mm; $n = 9$). The line corresponds to $W = 0.02L_b + 0.58$ ($n = 9$; $r^2 = 0.70$).

Results

Epifluorescence images revealed a regularly spaced rectangular feeding mesh (Fig. 2*A*) with a mean mesh width and length of $W = 1.5 \pm 0.5$ μm and $L = 6.0 \pm 1.5$ μm ($n = 9$; mean ± SD), respectively. Some strands were oriented obliquely or possibly tangled, but their number was small. Mesh width increased linearly with salp body length, L_b (Fig. 2*B*), as expected from an isometric scaling. The use of a rectangular rather than a square mesh is common among aquatic filter feeders, including appendicularians and caddisfly larvae, possibly optimizing the tradeoff between increasing encounter and lowering the mesh material and pressure drop (31).

Flow visualization provided both quantitative fluid speeds near the filter and a qualitative picture of the feeding current. The mean speed (U) and maximum speed near the oral siphon were 1.6 and 3.8 cm·s^{-1}, respectively (Table 1). The mean speed was slightly lower than speeds measured just aft of the atrial (excurrent) siphon using particle-image velocimetry (2.0–2.6 cm·s^{-1}) (32), likely because the oral siphon has a larger cross-sectional area. Particle trajectories showed that opening of the oral siphon resulted in the intake of fluid from around the edges of the siphon (Movie S1). Upon entering the pharyngeal chamber, water accelerated and then moved in a circular pattern, suggesting a tangential component of encounter between particles and the filter. The observed feeding current speeds are much higher than those of appendicularians (0.06–0.32 cm·s^{-1}) (17, 33), which pump fluid via sinusoidal motion of the tail, and doliolids (0.11 cm·s^{-1}) (34), which rely on cilia rather than muscles to draw fluid toward a mucous filter; and are of the same order as feeding currents of copepods and krill (0.6–1 cm·s^{-1}) (35, 36), which generate flow by the coordinated movement of feeding appendages. However, salps process much higher fluid volumes than crustaceans, due to the considerably larger cross-sections of their feeding currents.

Table 1. Flow speed at *P. confoederata* feeding filter

Individual	Stage	Body length, L_b, mm	Mean speed, U, cm·s^{-1} (n)	Max speed, cm·s^{-1}
1	Aggregate	27	2.3 ± 1.1 (3)	4.1
2	Solitary	30	1.2 ± 0.9 (9)	4.1
3	Solitary	34	1.5 ± 0.1 (15)	2.4
4	Solitary	53	1.9 ± 1.0 (13)	3.9
5	Solitary	56	2.0 ± 1.8 (11)	6.7
6	Solitary	62	0.8 ± 0.2 (14)	1.6
Mean ± SD (n)			1.6 ± 0.6 (6)	3.8 ± 1.7 (6)

Values expressed as mean ± SD. The mean speed weighted by the number of measurements for each organism was 1.5 ± 1.1 cm·s^{-1}. n, no. of measurements.

For example, grazing pressure by a bloom of the salp *Salpa thompsoni* in the Southern Ocean was equivalent to more than 100% of daily primary production, whereas grazing by dominant copepod species was negligible (37).

Both diffusional deposition and direct interception play a role in determining particle encounter by the filtering mesh, but direct interception is dominant for particle sizes $d_P > 0.05$ μm (Fig. 3). For $d_P = 0.01$–0.05 μm (viruses, colloids), diffusion is the primary mechanism of particle encounter, although efficiency is <2%. For the smallest particles, Brownian motion results in higher encounters compared with motility, whereas for $d_P > 0.2$ μm, diffusional deposition is larger for motile microorganisms. However, swimming is unlikely for organisms smaller than 0.6 μm, as Brownian rotation would turn them too frequently for swimming to be effective (39). For $d_P > 0.05$ μm, particles are more efficiently encountered via direct interception: for 0.5-μm nonmotile particles, encounter by direct interception is 254-fold higher than by diffusional deposition, and for 1-μm motile particles, that increase is 41-fold.

Because there are substantially higher numbers of small particles in the ocean (Fig. 1*B*), these particles can be disproportionately ingested even when encounter efficiencies are relatively low. Estimates of particle encounter based on encounter efficiency (Fig. 3) and realistic particle concentrations (Fig. 1*B*) show that, on average, particles in the 0.01- to 0.1-μm size range (viruses, colloids) are encountered at ~200× the rate of particles in the 0.1- to 1-μm range (submicron particles, bacteria, *Prochlorococcus*; Fig. 4*A*). However, larger particles still contribute more volume and carbon (Fig. 4*B*). The mean carbon contribution from 0.1- to 1-μm particles is 38× larger than from 0.01- to 0.1-μm particles. However, 1- to 10-μm particles contribute just 4× as much carbon as 0.1- to 1-μm particles (Fig. 4*B*). If only the outer 0.1 μm of each particle is digested, the situation is reversed: the 0.1- to 1-μm size range contributes 20% more carbon than the 1- to 10-μm range, and the maximum carbon contribution comes from 1.1-μm particles (Fig. 4*B*).

The model shows that particles smaller than the mesh width, $W = 1.4$ μm, supply a total of 0.15 $mg_C \cdot h^{-1}$ to a salp. The carbon ingestion rate of a 40-mm-long *P. confoederata* is 2.2% of the body carbon content each hour (41), or 0.02 $mg_C \cdot h^{-1}$ based on the carbon-to-body-length relationship of Madin et al. (42). Therefore, even assuming that the sticking coefficient is small (α = 0.1–0.2), the carbon supplied by particles smaller than the mesh opening can support the majority or entirety of the organism's carbon requirement.

To support this conclusion, predicted encounter rates via direct interception were tested experimentally by offering particles of three sizes (d_P = 0.5, 1, and 3 μm) to freshly collected *P. confoederata* and quantifying the relative capture rate of particles of each size. The particle size range where diffusional deposition is predicted to contribute significantly to encounter rates ($d_P < 0.05$; Fig. 3) was not tested in experiments, but its contribution in terms of carbon supply was predicted to be negligible based on model results (Fig. 4). When the same concentration of each particle size was offered, capture rates were similar among sizes, with a slight preference for the larger particles (Fig. 5*A*). Relative capture rates were 29.1 ± 8.6%, 30.1 ± 5.4%, and 40.8 ± 12.9% (mean ± SD) for 0.5-, 1-, and 3-μm particles, respectively. They were in general agreement with relative encounter rates from direct interception (relevant for particles >0.05 μm; Fig. 3), predicted to be 13.8%, 32.9%, and 53.3%, respectively. The discrepancy at the smallest size suggests that the contribution of smaller particles is even more pronounced than the model predicts. A model of simple sieving (17, 43) was an inferior predictor of relative encounter rates and was particularly poor at predicting encounter rates of the smallest particles, with mean relative encounter rates of 3.7%, 14.5%, and 81.9% for d_P = 0.5, 1, and 3 μm, respectively.

Offering a suspension of particles skewed toward higher concentrations at the smallest sizes confirmed these findings: measured rates were similar to those predicted by the direct interception model, and very different from the simple sieving model (Fig. 5*B*). In this case also, experiments showed an even higher capture rate of smaller particles than anticipated from modeled encounter rates. This difference could be due to a size dependence of the sticking coefficient α, for example, due to larger drag forces experienced by larger particles (44).

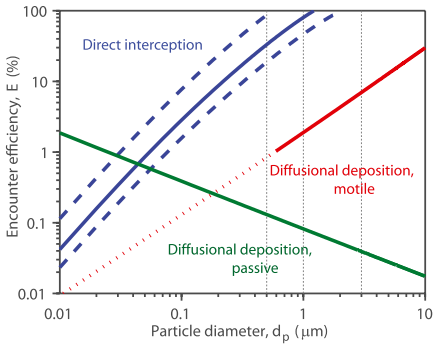

Fig. 3. Particle encounter efficiency predicted for *P. confoederata* over a range of particle sizes. Efficiency of direct interception (blue) is shown for the mean measured mesh width $W = 1.4$ μm (solid line), with lower and upper bounds (dashed lines) corresponding to minimum and maximum mesh widths ($W = 0.5$ and 2.3 μm, respectively; Fig. 2*B*). Efficiency of diffusional deposition is shown in green for passive particles and in red for motile microorganisms, with diffusivities from Visser and Kiørboe ($D = 2.8 d_p^{1.71}$, D in $cm^2 \cdot s^{-1}$, and d_P in cm) (38) for the latter. The red line is dashed for $d_p < 0.6$ μm because motility is unlikely for organisms of that size (39). Vertical gray dotted lines correspond to experimental particle sizes.

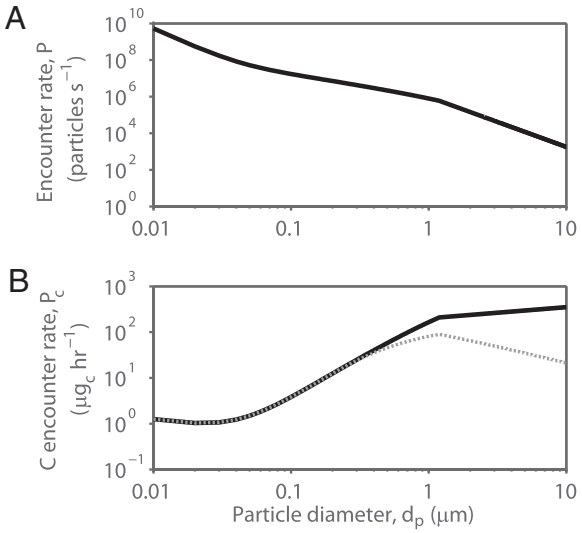

Fig. 4. Combined encounter rate predicted for direct interception and diffusional deposition (passive and motile particles) as a function of particle diameter for *P. confoederata*. Calculation based on Eq. **1**, with E from Fig. 3; $Q = 1.69$ mL·s^{-1} and $\log_{10} C = -0.91 \log_{10}(d_P^3 \pi/6) + 3.5$ (28) (Fig. 1). (*A*) Particle encounter rate and (*B*) carbon encounter rate based on $C_C = 0.11 V^{0.99}$, where C_C is carbon content (pg$_C$ $cell^{-1}$), and V is particle volume (μm^3) (40). For the latter, two cases were considered: that the full particle is digested (solid line) or that only the outer 0.1-μm-thick shell of each particle is digested (dashed line). Note that above $d_P = 1.2$ μm, direct interception efficiency is 100%.

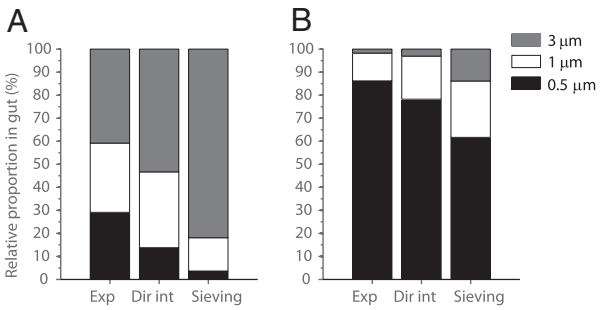

Fig. 5. Relative proportions of 0.5-, 1-, and 3-μm microspheres in *P. confoederata* gut after feeding experiments (Exp), compared with relative proportions predicted by direct interception (Dir int) and simple sieving (Sieving). (*A*) Equal initial concentrations of each particle size class (~10^3 particles mL^{-1}). (*B*) Higher initial concentration of smaller particles (0.5-, 1-, and 3-μm particle concentrations were ~10^5, ~10^4, and ~10^3 particles·mL^{-1}, respectively).

Discussion

Taken together, these findings suggest that simple sieving is not the sole feeding mechanism for salps, and instead that low Reynolds-number filtering mechanisms play a major and possibly dominant role by enabling salps to capture submicrometer particles. This is in stark contrast to previous results, which found that salp filter feeding was characterized by a size cutoff of 1–2 μm (2, 10). Particles smaller than the mesh opening W were considered unimportant for feeding in view of their negligible sieving efficiency, yet direct verification was hampered by measurement sensitivity (2, 10). Our model results show that diffusional deposition allows encounter of the smallest particles ($d_P < 0.05$ μm), although very inefficiently (Fig. 3). However, a large fraction of submicrometer particles (0.05 μm < $d_P < W$) can be efficiently encountered by direct interception (Fig. 4) and can largely or entirely satisfy salps' energetic requirements even if the sticking coefficient α is as small as 0.1.

If particles were fully digested, the majority of carbon would be supplied by particles in the 1- to 10-μm range (flagellates, small diatoms), which are primarily encountered by simple sieving, still with a significant contribution of 0.1- to 1-μm particles (bacteria, *Prochlorococcus*) encountered by direct interception. Contents of fecal pellets indicate that digestion of particles as small as 1 μm is partial (3, 4), and when digestion is limited to the outer shell of the particles (e.g., 0.1 μm), submicrometer particles can represent the majority of the carbon supply. The thinner the digested shell, the larger the contribution of smaller particles, because the nutritional value of larger particles now scales with their surface area (~d_P^2), rather than volume (~d_P^3). The particle size range providing the largest carbon contribution, then, results from a tradeoff between particle abundance decreasing, and volume increasing, with particle size. Yet, more experiments are required to quantify the degree of digestion of various particle types and the nutritional value of the digested fraction, especially considering the role of morphological and chemical properties of particle coating (labile organic coatings vs. cell walls, exoskeletons, plates, spines).

The model calculations presented here rely on a relation for carbon content originally developed for phytoplankton ($2 < d_P <$ 60 μm) (40). It is thus important to establish whether the carbon content of micrometer- and submicron-scale particles in the ocean is consistent with this assumption. Of particular interest is the carbon content of marine colloids, which are highly abundant particles in the 1 nm to 1 μm range, constituting 30–50% of dissolved organic carbon (DOC) in the upper ocean (45). These particles originate from biological processes, including cell exudation (e.g., transparent exopolymers), viral infection, autolysis, egestion by flagellates, and sloppy feeding (46). Thus, labile colloidal components can be rich in polysaccharides, proteins, and lipids (46, 47), and can play an important role in biogeochemical processes (48–50). Although a conclusive understanding of the bioavailability of colloidal particles remains a major frontier for biogeochemists, work conducted in several aquatic ecosystems has shown that colloids are 6–37% organic carbon (median = 27%) (47). This finding is consistent with, and even somewhat on the larger side of, the figure for carbon content used here [~11%, based on $C_C = 0.11V^{0.99}$ (40) and a colloid density of ~1 g·mL^{-1} (51)]. Regardless of the nutritional value, salps influence the turnover of the colloidal fraction of DOC through encounter and, ultimately, assimilation or defecation.

Salp filtration rates are among the highest in the ocean, reaching up to 15.3 mL·s^{-1} (2, 52), yet pelagic tunicates have among the smallest diameter mesh elements (see figure 6 in ref. 53) and mesh spacing (10) of all marine filter feeders. By constantly pumping large volumes of seawater through their bodies and retaining micrometer scale and submicrometer particles, salps are well adapted for existence in the oligotrophic ocean. Most salp species are more oceanic than neritic in distribution, and high particle concentrations in coastal areas can clog their filtering apparatus and disrupt feeding (54). Oceanic waters are frequently dominated by plankton that is too small to be captured by sieving. The finding that salps can fulfill their energetic requirements with only submicrometer particles helps explain this geographic distribution.

Carbon in the euphotic zone is typically regenerated on the order of hours via the microbial loop (55). Salps and other pelagic tunicates remove particles that are four to five orders of magnitude smaller than themselves, thereby bypassing several trophic levels (55). In addition, muscular pumping achieves a high throughput of seawater and associated particles compared with the much slower feeding currents generated by flagella or cilia in other planktonic filter feeders. Particles are packaged into membrane-bound fecal pellets that are often incompletely digested and therefore rich in carbon, nitrogen, and phosphorous (56), and contain trace elements (e.g., Ca and Mg) (4). Fecal pellets sink quickly and are transferred to a longer-lived pool in deeper water, where material is sequestered on time scales of years to centuries. The efficiency with which salps repackage and export carbon from surface waters suggests that salps, particularly in bloom proportions, can profoundly influence biogeochemical cycling, as indicated also by a recent proposition to increase global salp populations to mitigate climate change (57). In summary, the high filtration rates of small particles imply that salps can rapidly transfer carbon and energy from the submicron size range of the particle spectrum to higher trophic levels by grazing, and to larger depths via their rapidly sinking fecal pellets. As such, salps can provide a substantial shortcut to flocculation in determining the contribution of small particles to vertical transport of particulate matter.

Materials and Methods

Specimen Collection. *Pegea confoederata* were collected in individual 800-mL plastic jars using blue-water SCUBA techniques (58) at the Liquid Jungle Lab off the Pacific coast of Panama (7° 50′ N, 81° 35′ W) during January 2007, 2008, and 2009. Animals were maintained in collection jars or in tanks (6–11 L) of field-collected seawater at in situ temperatures (26–28 °C). All measurements were made within 12 h of collection.

Measurements of Mesh Size and Flow Speed. Filter mesh measurements were obtained by epifluorescence microscopy. Part of the mesh of *P. confoederata* was removed by gently inserting an ~1 × 1-mm section of a glass coverslip through the oral siphon and sweeping it through the pharyngeal chamber using forceps. After adding 50–100 μL of lectin-fluorescein isothiocyanate in seawater solution (1 mg·mL^{-1}), the mesh was imaged using a Zeiss Axiostar Plus microscope with an HBO 50 epifluorescence lamp, a 100× objective, and a Nikon Coolpix 8800 camera. This is the first time the filtering mesh was imaged using a wet preparation to reduce sample distortion caused by drying and shrinking associated with TEM and SEM techniques (3, 59). Data were

acquired from six *P. confoederata* solitaries and three aggregates, ranging from 16 to 60 mm long. Mesh length, *L*, and width, *W*, were measured in ImageJ (http://rsbweb.nih.gov/ij/) for multiple mesh openings (mean ± SD = 16 ± 10) and averaged for each individual.

The flow pattern and speed were determined using particle tracking. Individual *P. confoederata* were placed in custom-built acrylic tanks with field-collected seawater seeded with 10 ± 2 μm titanium dioxide particles. Particles were illuminated with a 1-mm-thick laser sheet (30 mW, 500 nm wavelength) generated using a Powell lens (Lasiris) and their motion videotaped with a Sony HDR-HC7 videocamera (1,440 × 1,080 pixels, 30 fps). Because salps are transparent, particles could be tracked within the pharyngeal chamber until contact with the filtering mesh occurred. Velocities were determined by tracking individual particles between frames relative to landmarks on the salp body or by measuring particle streak lengths in a single frame using ImageJ.

Particle Encounter Model. The encounter rate (60)

$$P = \beta C = EQC \left(\text{particles s}^{-1}\right) \quad [1]$$

is the product of the encounter rate kernel, β (mL·s^{-1}), and the particle concentration, *C* (particles mL^{-1}). Here, β = *EQ*, where *E* (dimensionless) is the capture efficiency (*SI Appendix*) and *Q* (mL·s^{-1}) is the volume flow rate through the salp. Both *E* and *C* depend on particle diameter, d_P. Particle capture by salps is a low Re-number process, indicating that viscous forces dominate inertial forces in determining capture. The flow through the mesh has Re = $WU/\nu \sim 3 \times 10^{-2}$, and the flow around an individual mesh strand (diameter $d \sim 0.1$ μm) (10) has Re = $dU/\nu \sim 2 \times 10^{-3}$. Particle inertia is negligible, as the Stokes number $d_P^2 U \rho_p / 18 \rho \nu d$ is always <1 for $d_P < 10$ μm, particle density ρ_p = 1,037 kg·m^{-3}, and seawater density ρ = 1,030 kg·m^{-3}. Thus, particle capture is limited to noninertial mechanisms, which include direct interception and diffusional deposition (12).

We used a model for capture efficiency, *E*, by a rectangular mesh (*SI Appendix*) (12), with parameters that were directly measured (mesh dimensions, flow through the filter) or taken from literature (mesh fiber diameter, particle size distribution). We assumed spherical particles in Eq. **1**. The encounter of nonmotile and motile particles by diffusional deposition was modeled by a diffusivity based on Brownian motion and random motility, respectively (*SI Appendix*).

The volume flow rate through the salp, *Q* = 1.69 mL·s^{-1}, was determined as the average from three studies (20, 52, 61) and had an SD of 1.44 mL·s^{-1}. The particle size distribution, concentration *C* of particles of size d_P, was obtained from four Atlantic Ocean transects (28) and is likely a conservative estimate, as other studies found higher concentrations in all size ranges (Fig. 1*B*). Carbon encounter was calculated using the relation $C_C = 0.11V^{0.99}$ (40) between carbon content, C_C (pg$_C$ cell^{-1}), and particle volume, *V* (μm^3), for phytoplankton (similar relations apply for bacterioplankton and colloids) (47, 62). Because partially undigested particles are frequently observed in salp fecal pellets (3, 4), we also explored the implications for carbon encounter if only the outer 0.1 μm of each particle is digested. Relative estimates of particle and carbon encounters mentioned in the text were computed based on uniformly distributed values of particle diameter with spacing of 0.01 μm.

Particle Capture Experiments. Relative retention efficiencies of d_P = 0.5-, 1-, and 3-μm fluorescent polystyrene microspheres (Polysciences, Inc.) were determined using two feeding experiments, performed within 3 h of specimen collection. Microspheres were pretreated with 5 mg·mL^{-1} BSA for 12–48 h to avoid clumping (63). In the first experiment, microspheres were added to each jar at a concentration $C \approx 10^3$ mL^{-1} for each size. After 2 h, *P. confoederata* guts were excised and ground using a mortar and pestle along with several microliters of seawater. Two 2-μL subsamples of the homogenate were examined using epifluorescence microscopy at 200× magnification and 365 ± 12 nm excitation, and particles of each size were counted from three fields of view from each 2-μL subsample. The three particle sizes were distinguished based on size (d_P = 0.5, 1, and 3 μm) and emission wavelength (486, 407, and 486 nm, respectively). Each count included a minimum of 50 particles. In the second experiment the starting concentrations were $C \approx 10^5$, 10^4, and 10^3 mL^{-1} for d_P = 0.5, 1, and 3 μm, respectively, to better represent the prevalence of small particles in the ocean (Fig. 1*B*). For both experiments, relative retention efficiencies were determined by dividing the count for a given particle size by the total count for all three sizes. Comparisons were made between relative retention efficiencies from experiments, the low-Re encounter model, and a simple sieving model based on an experimentally determined Gaussian distribution of mesh widths (17, 43).

ACKNOWLEDGMENTS. We thank those who facilitated our work at the Liquid Jungle Lab, Panama, especially Ellen Bailey, Luis Camilli, and numerous SCUBA divers. Mark Wells, Hugh Ducklow, and Dariusz Stramski, as well as two anonymous reviewers, provided insightful comments relating to the manuscript. This work was supported by National Science Foundation Grants OCE-0647723 (to L.P.M.) and OCE-074464-CAREER (to R.S.) and the Woods Hole Oceanographic Institution Ocean Life Institute.

1. Alldredge AL, Madin LP (1982) Pelagic tunicates: Unique herbivores in the marine plankton. *Bioscience* 32:655–663.
2. Madin LP, Deibel D (1998) *The Biology of Pelagic Tunicates*, ed Bone Q (Oxford Univ Press, New York), pp 81–103.
3. Silver MW, Bruland KW (1981) Differential feeding and fecal pellet composition of salps and pteropods, and the possible origin of deep water flora and olive-green "cells". *Mar Biol* 62:263–273.
4. Caron DA, Madin LP, Cole JJ (1989) Composition and degradation of salp fecal pellets: Implications for vertical flux in oceanic environments. *J Mar Res* 47:829–850.
5. Yoon WD, Marty JC, Sylvain D, Nival P (1996) Degradation of fecal pellets in *Pegea confoederata* (Salpidae, Thaliacea) and its implication in the vertical flux of organic matter. *J Exp Mar Biol Ecol* 203:147–177.
6. Phillips B, Kremer P, Madin LP (2009) Defecation by *Salpa thompsoni* and its contribution to vertical flux in the Southern Ocean. *Mar Biol* 156:455–467.
7. Madin LP, et al. (2006) Periodic swarms of the salp *Salpa aspera* in the Slope Water off the NE United States: Biovolume, vertical migration, grazing and vertical flux. *Deep Sea Res Part I Oceanogr Res Pap* 53:804–819.
8. Wiebe PH, Madin LP, Haury LR, Harbison GR, Philbin LM (1979) Diel vertical migration by *Salpa aspera* and its potential for large-scale particulate organic matter transport to the deep-sea. *Mar Biol* 53:249–255.
9. Rubenstein DI, Koehl MAR (1977) The mechanisms of filter feeding: Some theoretical considerations. *Am Nat* 111:981–994.
10. Bone Q, Carre C, Chang P (2003) Tunicate feeding filters. *J Mar Biol Assoc UK* 83: 907–919.
11. Shimeta J, Jumars PA (1991) Physical mechanisms and rates of particle capture by suspension feeders. *Oceanogr Mar Biol* 29:191–257.
12. Silvester NR (1983) Some hydrodynamic aspects of filter feeding with rectangular mesh nets. *J Theor Biol* 103:265–286.
13. Loudon C, Alstad DN (1990) Theoretical mechanics of particle capture: Predictions for hydropsychid caddisfly distributional ecology. *Am Nat* 135:360–381.
14. Deibel D, Lee SH (1992) Retention efficiency of submicrometer particles by the pharyngeal filter of the pelagic tunicate *Oikopleura vanhoeffeni*. *Mar Ecol Prog Ser* 81:25–30.
15. Flood PR, Deibel D, Morris CC (1992) Filtration of colloidal melanin from seawater by planktonic tunicates. *Nature* 355:630–632.
16. Fernández D, Lopez-Urrutia A, Fernández A, Acuña JL, Harris R (2004) Retention efficiency of 0.2 to 6 μm particles by the appendicularians *Oikopleura dioica* and *Fritillaria borealis*. *Mar Ecol Prog Ser* 266:89–101.
17. Acuña JL, Deibel D, Morris CC (1996) Particle capture mechanism of the pelagic tunicate *Oikopleura vanhoeffeni*. *Limnol Oceanogr* 41:1800–1814.
18. Shimeta J (1993) Diffusional encounter of submicrometer particles and small cells by suspension feeders. *Limnol Oceanogr* 38:456–465.
19. Kremer P, Madin LP (1992) Particle retention efficiency of salps. *J Plankton Res* 14: 1009–1015.
20. Harbison GR, Gilmer RW (1976) The feeding rates of the pelagic tunicate *Pegea confoederata* and two other salps. *Limnol Oceanogr* 21:517–528.
21. Fuhrman J (2000) *Microbial Ecology of the Oceans*, ed Kirchman DL (Wiley-Liss, New York), pp 327–350.
22. Wells ML, Goldberg ED (1994) The distribution of colloids in the North Atlantic and Southern Oceans. *Limnol Oceanogr* 39:286–302.
23. Yamasaki A, et al. (1998) Submicrometer particles in northwest Pacific coastal environments: Abundance, size distribution, and biological origins. *Limnol Oceanogr* 43:536–542.
24. Caron DA, et al. (1995) The contribution of microorganisms to particulate carbon and nitrogen in surface waters of the Sargasso Sea near Bermuda. *Deep Sea Res Part I Oceanogr Res Pap* 42:943–972.
25. Li WKW (1998) Annual average abundance of heterotrophic bacteria and *Synechococcus* in surface ocean waters. *Limnol Oceanogr* 43:1746–1753.
26. Partensky F, Hess WR, Vaulot D (1999) *Prochlorococcus*, a marine photosynthetic prokaryote of global significance. *Microbiol Mol Biol Rev* 63:106–127.
27. Dennett MR, et al. (1999) Abundance and biomass of nano- and microplankton assemblages during the 1995 Northeast Monsoon and Spring Intermonsoon in the Arabian Sea. *Deep Sea Res Part I Oceanogr Res Pap* 46:1691–1717.
28. Cermeño P, Figueiras FG (2008) Species richness and cell-size distribution: Size structure of phytoplankton communities. *Mar Ecol Prog Ser* 357:79–85.
29. Sheldon RW, Prakash A, Sutcliffe WH (1972) The size distribution of particles in the ocean. *Limnol Oceanogr* 17:327–340.
30. Wells ML, Goldberg ED (1991) Occurrence of small colloids in sea water. *Nature* 353: 342–344.

31. Wallace JB, Malas D (1976) The significance of the elongate, rectangular mesh found in capture nets of fine particle filter feeding trichoptera larvae. *Arch Hydrobiol* 77: 205–212.
32. Sutherland KR, Madin LP Jet wake structure and swimming performance of salps. *J Exp Biol*, in press.
33. Morris CC, Deibel D (1993) Flow rate and particle concentration within the house of the pelagic tunicate *Oikopleura vanhoeffeni*. *Mar Biol* 115:445–452.
34. Bone Q, Braconnot JC, Carre C, Ryan KP (1997) On the filter-feeding of Doliolum (Tunicata: Thaliacea). *J Exp Mar Biol Ecol* 214:179–193.
35. van Duren LA, Stamhuis EJ, Videler JJ (2003) Copepod feeding currents: Flow patterns, filtration rates and energetics. *J Exp Biol* 206:255–267.
36. Yen J, Brown J, Webster DR (2003) Analysis of the flow field of the krill, *Euphausia pacifica*. *Mar Freshwat Behav Physiol* 36:307–319.
37. Dubischar CD, Bathmann UV (1997) Grazing impact of copepods and salps on phytoplankton in the Atlantic sector of the Southern Ocean. *Deep Sea Res Part II Top Stud Oceanogr* 44:415–433.
38. Visser AW, Kiørboe T (2006) Plankton motility patterns and encounter rates. *Oecologia* 148:538–546.
39. Dusenbery DB (2009) *Living at the Micro Scale: The Unexpected Physics of Being Small* (Harvard Univ Press, Cambridge, MA).
40. Montagnes DJS, Berges JA, Harrison PJ, Taylor FJR (1994) Estimating carbon, nitrogen, protein, and chlorophyll *a* from volume in marine phytoplankton. *Limnol Oceanogr* 39:1044–1060.
41. Cetta CM, Madin LP, Kremer P (1986) Respiration and excretion by oceanic salps. *Mar Biol* 91:529–537.
42. Madin LP, Cetta CM, McAlister VL (1981) Elemental and biochemical composition of salps (Tunicata:Thaliacea). *Mar Biol* 63:217–226.
43. Harbison GR, McAlister VL (1979) The filter-feeding rates and particle retention efficiencies of three species of *Cyclosalpa* (Tunicata, Thaliacea). *Limnol Oceanogr* 24: 875–892.
44. Shimeta J, Koehl MAR (1997) Mechanisms of particle selection by tentaculate suspension feeders during encounter, retention, and handling. *J Exp Mar Biol Ecol* 209:47–73.
45. Guo LD, Coleman CH, Santschi PH (1994) The distribution of colloidal and dissolved organic-carbon in the Gulf of Mexico. *Mar Chem* 45:105–119.
46. Nagata T, Kirchman DL (1997) *Advances in Microbial Ecology*, ed Jones G (Plenum, New York), pp 81–103.
47. Guo L, Santschi PH (1997) Composition and cycling of colloids in marine environments. *Rev Geophys* 35:17–40.
48. Amon RMW, Benner R (1994) Rapid cycling of high-molecular-weight dissolved organic matter in the ocean. *Nature* 369:549–552.
49. Verdugo P, et al. (2008) Marine biopolymer self-assembly: Implications for carbon cycling in the ocean. *Faraday Discuss* 139:393–398, discussion 399–417, 419–420.
50. Wells ML (2002) *Biogeochemistry of Marine Dissolved Organic Matter*, eds Hansell DA, Carlson CA (Elsevier Science, London), pp 367–404.
51. Dean RB (1948) *Modern Colloids: An Introduction to the Physical Chemistry of Large Molecules and Small Particles* (Van Nostrand, New York).
52. Sutherland KR, Madin LP (2010) A comparison of filtration rates among pelagic tunicates using kinematic measurements. *Mar Biol* 157:755–764.
53. Humphries S (2009) Filter feeders and plankton increase particle encounter rates through flow regime control. *Proc Natl Acad Sci USA* 106:7882–7887.
54. Harbison GR, McAlister VL, Gilmer RW (1986) The response of the salp, *Pegea confoederata*, to high levels of particulate material: Starvation in the midst of plenty. *Limnol Oceanogr* 31:371–382.
55. Fortier L, Lefevre J, Legendre L (1994) Export of biogenic carbon to fish and to the deep-ocean: The role of large planktonic microphages. *J Plankton Res* 16:809–839.
56. Andersen V (1998) *The Biology of Pelagic Tunicates*, ed Bone Q (Oxford Univ Press, New York), pp 125–137.
57. Kithil PW. Are salps a silver bullet against global warming and ocean acidification? American Geophysical Union Fall Meeting, December 11-15, 2006, abst OS21A-1571. Available at http://adsabs.harvard.edu/abs/2006AGUFMOS21A1571K.
58. Haddock SHD, Heine JN (2005) *Scientific Blue-Water Diving* (California Sea Grant College Program, La Jolla, CA), Report T-057.
59. Bone Q, Braconnot JC, Ryan KP (1991) On the pharyngeal feeding filter of the salp *Pegea confoederata* (Tunicata, Thaliacea). *Acta Zool* 72:55–60.
60. Kiørboe T (2008) *A Mechanistic Approach to Plankton Ecology* (Princeton Univ Press, Princeton, NJ).
61. Madin LP, Kremer P (1995) Determination of the filter-feeding rates of salps (Tunicata, Thaliacea). *ICES J Mar Sci* 52:583–595.
62. Posch T, et al. (2001) Precision of bacterioplankton biomass determination: A comparison of two fluorescent dyes, and of allometric and linear volume-to-carbon conversion factors. *Aquat Microb Ecol* 25:55–63.
63. Pace ML, Bailiff MD (1987) Evaluation of a fluorescent microsphere technique for measuring grazing rates of phagotrophic microorganisms. *Mar Ecol Prog Ser* 40: 185–193.